

Adsorption of cationic dye on *N,O*-carboxymethyl-chitosan from aqueous solutions: equilibrium, kinetics, and adsorption mechanism

Li Wang · Qi Li · Aiqin Wang

Received: 6 April 2010 / Revised: 31 July 2010 / Accepted: 31 July 2010 /
Published online: 13 August 2010
© Springer-Verlag 2010

Abstract In order to improve the adsorption capacity of chitosan (CTS) for methylene blue (MB) cationic dye, a series of *N,O*-carboxymethyl-chitosans (*N,O*-CMCTS) were prepared under heterogeneous conditions by controlling the reaction time. The adsorption of MB from aqueous solution onto *N,O*-CMCTS was studied. The effects of degree of substitution (DS) of *N,O*-CMCTS, initial pH of the dye solution and adsorption temperature were investigated in detail. The results showed that the adsorption capacities of *N,O*-CMCTS increased with the increase of DS and *N,O*-CMCTS with DS of 0.72 exhibited the highest adsorption capacity (349 mg/g). The adsorption kinetics of *N,O*-CMCTS was found to follow the pseudo-second-order model. The adsorption equilibrium of *N,O*-CMCTS fitted very well with the Langmuir isotherm model, showing maximum monolayer adsorption capacity of 351 mg/g. The adsorption mechanism of *N,O*-CMCTS was also discussed by means of FTIR spectra and XPS. The results revealed that the –OH, –NH₂, and –COOH groups of *N,O*-CMCTS were involved in the adsorption process. The desorption studies showed that *N,O*-CMCTS could be regenerated and used for the adsorption of MB repeatedly.

Keywords *N,O*-carboxymethyl-chitosan · Adsorption · Methylene blue · Equilibrium · Kinetics · Mechanism

L. Wang (✉) · Q. Li
College of Material Science and Art Design, Inner Mongolia Agricultural University, Hohhot
010018, People's Republic of China
e-mail: wl2083663@126.com

A. Wang
Center of Eco-Material and Green Chemistry, Lanzhou Institute of Chemical Physics, Chinese
Academy of Sciences, Lanzhou 730000, People's Republic of China

Introduction

Pigments and dyes are widely used in the textile and leather dyeing, paper, printing, pharmaceutical, and cosmetic industries. A large amount of aqueous waste and dye effluents with strong persistent color and high biochemical oxygen demand (BOD), over $4.4 \times 10^6 \text{ m}^3$ per day in Mainland China [1], is discharged from the dyeing process, which is esthetically and environmentally unacceptable [2]. Therefore, dye removal has been an important but challenging area of wastewater treatment.

It is difficult to remove the dyes from the effluent because the dyes are stable to light and heat, and are biologically non-degradable [3]. Various treatment techniques including coagulation and flocculation [4], membrane separation [5, 6], oxidation or ozonation [7, 8], electro-coagulation [9], and adsorption [10, 11], have been used for the removal of colored dyes from wastewater. Adsorption is a well-established separation technique to remove dilute pollutants as well as to recover valuable products from aqueous streams [12]. It has been reported that many different types of adsorbents are effective in removing color from aqueous effluent. Considerable attention has been drawn to natural polymeric materials over the past decade because of their biodegradable and non-toxic nature [13]. Chitosan (CTS) is the *N*-deacetylated derivative of chitin and the second most plentiful natural biopolymer. As a well-known adsorbent, CTS is widely used for the removal of heavy, transition metals and dyes [14–16]. However, its application for the adsorption of cationic dyes such as methylene blue (MB) is seldom reported because it is a natural cationic polysaccharide.

The last decade has witnessed a growing interest in chemical modification of CTS and its derivatives to enhance their properties and consequently expand their potential applications [17–22]. Among various techniques for chemical modifications, carboxymethylation is very attractive. It introduces active hydroxyl (–OH), carboxyl (–COOH), and amine (–NH₂) groups into the molecule, which make it possible to increase adsorption capacity for heavy, transition metals [23–26] and dyes [27]. However, to the best of our knowledge, the adsorption of *N,O*-carboxymethyl-chitosans (*N,O*-CMCTS) for MB cationic dye has not been reported up to now. Therefore, the aim of this study was to investigate the adsorption behavior of *N,O*-CMCTS for MB dye in detail. The effects of degree of substitution (DS) of *N,O*-CMCTS, initial pH of the dye solution and adsorption temperature were investigated. The adsorption kinetics and isotherms for MB dye onto *N,O*-CMCTS were studied. The adsorption mechanism of *N,O*-CMCTS for MB was also discussed by means of FTIR spectra and XPS.

Experimental

Materials

The degree of deacetylation and viscosity average molecular weight of CTS (Zhejiang Yuhuan Ocean Biology Co., China) are 85% and 9.0×10^5 , respectively. Monochloroacetic acid was purchased from Tianjin Chemical Reagent Co., China. The molecular formula of MB (Shanghai Reagent Corp., China) is C₁₆H₁₈N₃SCl.

Other agents used were all of analytical grade and all solutions were prepared with distilled water.

Preparation of *N,O*-CMCTS

N,O-CMCTS with different DS were prepared according to our previous report [27]. CTS (5.00 g) was added to a 20 wt% sodium hydroxide solution (50.00 mL) for 12 h at room temperature, and then separated by filtration. The treated CTS was dipped into 50 mL of 100% (v/v) anhydrous alcohol in a three-necked flask with stirring for 30 min at room temperature, and then monochloroacetic acid (3.58 g) was added into the reaction mixture and stirred for additional 30 min. Then the mixture was heated to 60 °C and allowed to continue for the predetermined time (15, 30, 60, 90, 120 min). Finally, the resultant solution was filtered and the filter cake was dissolved in distilled water. The solution obtained was adjusted to pH 7.0 and precipitated by pouring into 100% (v/v) anhydrous alcohol. The white precipitate was filtered, washed with 70% (v/v) ethanol for three times and 100% (v/v) anhydrous alcohol once, and then dried under vacuum at 80 °C to obtain the products. The DS of *N,O*-CMCTS was determined using potentiometric titration [28]. The point of zero charge (pH_{PZC}) of samples was determined by the solid addition method [29]. The properties of CTS and *N,O*-CMCTS are shown in Table 1.

Characterization

FTIR spectra of the samples were carried out using a FTIR spectrophotometer (Thermo Nicolet, NEXUS, TM) in KBr pellets. Micrographs of the samples were taken using SEM (JSM-6701F, JEOL, Ltd.). Before observation of SEM, all samples were fixed on aluminum stubs and coated with gold. XPS spectra of the samples were performed using an X-ray photoelectron spectrometer (VG Scientific Escalab 210-UK) with a twin anode (Mg Ka/Al Ka), scanning at 6.80 ms/step, 0.6 eV/step, and 6 sweeps.

Adsorption experiments

All batch experiments were performed on a thermostated shaker (THZ-98A) at 120 rpm. The effect of DS on dye removal was carried out in 25 mL of the dye

Table 1 The properties of CTS and *N,O*-CMCTS

Samples	DS	Density (g mL^{-1})	pH_{PZC}	Color
CTS	0	0.33	6.3	White
<i>N,O</i> -CMCTS	0.32	0.35	7.3	Light yellow
<i>N,O</i> -CMCTS	0.57	0.40	7.5	Light yellow
<i>N,O</i> -CMCTS	0.76	0.42	7.8	Light yellow
<i>N,O</i> -CMCTS	0.89	0.43	8.0	Light yellow
<i>N,O</i> -CMCTS	0.95	0.44	8.1	Light yellow

solutions (1600 mg/L, pH = 8.0) with 0.10 g of adsorbent at 30 °C for 60 min. The influence of pH on MB removal was studied by adjusting MB solutions (1600 mg/L) to different pH (2.0, 3.0, 4.0, 5.0, 6.0, 7.0, 8.0, 9.0, and 10.0) using a pH meter (DELTA-320) and agitating 25 mL of dye solution with 0.10 g of adsorbent at 30 °C for 60 min. The effect of temperature on dye removal was carried out in 25 mL of the dye solutions (1800 mg/L, pH 8.0) with 0.10 g of adsorbent for 60 min.

For kinetic studies, 1600 mg/L dye solutions (25 mL, pH 8.0) were agitated with 0.10 g of adsorbent at 30 °C for predetermined intervals of time. Batch equilibrium adsorption experiments were carried out by agitating 25 mL MB solution of various concentrations at pH = 8.0 with 0.10 g of adsorbent at 30 °C until equilibrium was established.

The samples were withdrawn from the shaker at predetermined time intervals and the dye solution was separated from the adsorbent by centrifugation at 4500 rpm for 10 min. The absorbencies of samples were measured using a UV–vis spectrophotometer (Specord 200) at wavelength 670 nm (MB has a maximum absorbency at wavelength 670 nm on a UV–vis spectrophotometer). Then, the concentrations of the samples were determined by using linear regression equation ($y = 0.1751x - 0.1145$, $R^2 = 0.9998$) obtained by plotting a calibration curve for dye over a range of concentrations. The amounts of MB adsorbed onto samples were calculated by subtracting the final solution concentration from the initial concentration of dye solutions.

Desorption studies

For batch desorption study, the adsorbent utilized for the adsorption of an initial dye concentration of 1600 mg/L was separated from the dye solution by centrifugation. The dye-loaded adsorbent was washed gently with water to remove any unadsorbed dye. Then, the spent adsorbent was stirred using a magnetic stirrer with 25 mL of distilled water at different pHs for 60 min. The desorbed dye was determined as mentioned before.

Results and discussion

FTIR analysis of *N,O*-CMCTS

The FTIR spectra of CTS (a) and *N,O*-CMCTS (b) are shown in Fig. 1. As can be seen, the absorption band at 3444 cm^{-1} , corresponding to the stretching vibrations of O–H and N–H groups of CTS, is widened and weakened after carboxymethylation. The stretching vibration of the NH–CO (I) group (1640 cm^{-1}), the bending vibration of N–H group (1599 cm^{-1}), and the stretching vibration of the O–H group (1032 cm^{-1}) of CTS disappeared. In addition, the characteristic absorption bands of the asymmetric and symmetric stretching vibrations of COO^- (1600 cm^{-1} and 1412 cm^{-1}) were observed in the spectrum of *N,O*-CMCTS. The information observed from FTIR spectra indicates that carboxymethylation has occurred on both

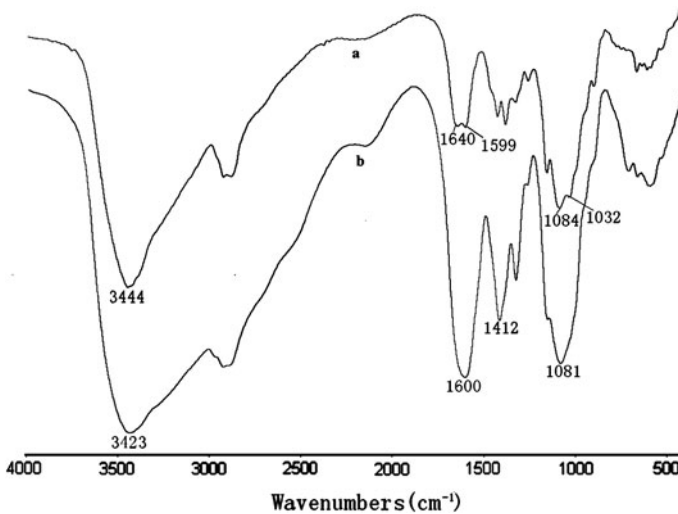


Fig. 1 IR spectra of CTS (a), *N,O*-CMCTS with the DS of 0.76 (b)

the amino and hydroxyl groups of CTS, which may have an influence on absorption properties of *N,O*-CMCTS.

SEM images analysis of *N,O*-CMCTS

The morphologies of CTS (a) and *N,O*-CMCTS (b) are shown in Fig. 2. It can be seen from this figure that CTS shows a tight and nonporous surface, but *N,O*-CMCTS has a relatively loose and fibrous surface, which may be convenient for the penetration of dye molecules into the *N,O*-CMCTS powder and result in an increase in the adsorption capacity of MB on *N,O*-CMCTS.

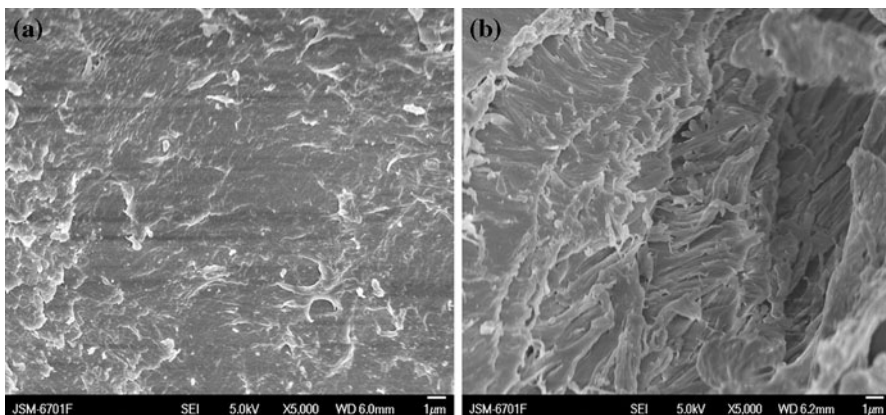


Fig. 2 SEM images of CTS (a), *N,O*-CMCTS with the DS of 0.76 (b)

Effect of DS of *N,O*-CMCTS on adsorption

The DS of *N,O*-CMCTS plays an extremely important role in the adsorption capacities of *N,O*-CMCTS. Figure 3 shows the effect of the DS on the adsorption capacities of *N,O*-CMCTS. As can be seen from this figure, CTS (DS = 0) has small adsorption capacity (36 mg/g) for MB. However, the adsorption capacity of *N,O*-CMCTS sharply increases from 190 to 349 mg/g with increasing the DS from 0.32 to 0.76. This is due to the fact that the chemical interaction and the electrostatic attraction may occur between $-\text{COOH}$ group of *N,O*-CMCTS and MB cationic dye. The results also show that the adsorption capacity of *N,O*-CMCTS slightly decreases from 349 to 336 mg/g with further increasing DS from 0.76 to 0.95. This observation may be interpreted as follows. On the one hand, excessive $-\text{COOH}$ group would lead to the increase of steric hindrance with the DS of *N,O*-CMCTS increasing. On the other hand, $-\text{NH}_2$ and $-\text{OH}$ groups of the repeated structure units of *N,O*-CMCTS decrease with increasing the DS, which result in a slight decrease of adsorption capacity of MB on *N,O*-CMCTS. It can be concluded from the above discussion that the adsorption sites of *N,O*-CMCTS may be not only the $-\text{COOH}$ group but also the $-\text{NH}_2$ and $-\text{OH}$ groups. This can be further proved by the changes in the FTIR spectra and XPS of *N,O*-CMCTS before and after dye adsorption, as will be described later in detail.

Effect of the pH on adsorption

The effect of pH on the adsorption capacity of *N,O*-CMCTS was shown in Fig. 4. It is evident that pH is an important factor influencing the adsorption capacity of *N,O*-CMCTS. As shown in Fig. 4, the adsorption capacity sharply increased from 158 to 349 mg/g as the pH of the solution was increased from 4.0 to 8.0, and then

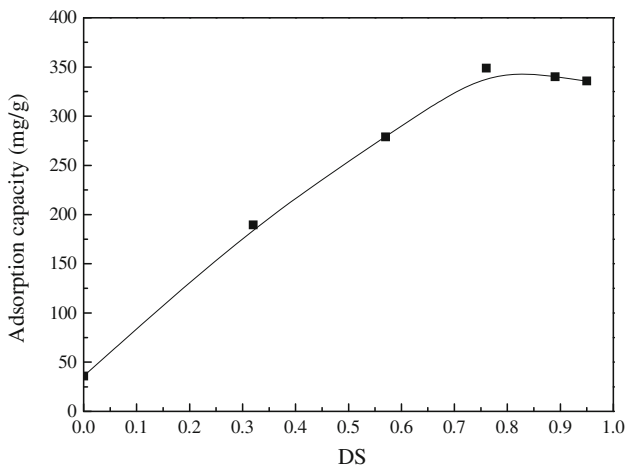


Fig. 3 Effect of the DS on the adsorption capacity of *N,O*-CMCTS for MB. Adsorption experiments—dye concentration: 1600 mg/L; sample dose: 0.10 g/25.00 mL; pH: 8.0; temperature: 30 °C; equilibrium time: 60 min

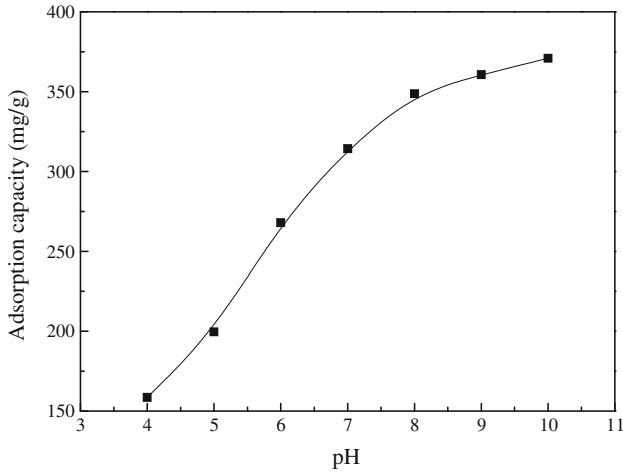
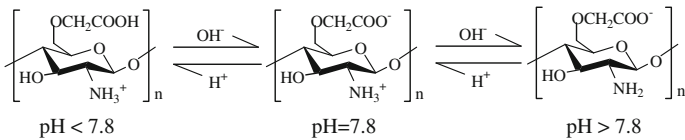


Fig. 4 Effect of the pH on the adsorption capacities of *N,O*-CMCTS with the DS of 0.76 for MB. Adsorption experiments—dye concentration: 1600 mg/L; sample dose: 0.10 g/25 mL; temperature: 30 °C; equilibrium time: 60 min

continuously increased from 349 to 371 mg/g with further increasing pH from 7.0 to 9.0. To understand the adsorption mechanism, it is necessary to determine the point of zero charge (pH_{PZC}) of the adsorbent [25]. Adsorption of cations is favored at $pH > pH_{PZC}$, while the adsorption of anions is favored at $pH < pH_{PZC}$ [30]. In this study, pH_{PZC} for *N,O*-CMCTS with DS of 0.76 is 7.8. Usually, as an amphoteric polyelectrolyte, *N,O*-CMCTS has a different structure in acidic and alkaline media and may be written as:



When the pH of MB dye solution is higher than 7.8, the *N,O*-CMCTS surface is negatively charged. Taking into account that MB is in the cationic form, the electrostatic interaction between *N,O*-CMCTS and MB facilitates an increase of dye adsorption. Nevertheless, significant adsorption still occurred at pH below pH_{PZC} due to the fact that a chemical interaction between MB dye and *N,O*-CMCTS took place, which will be discussed in the adsorption mechanism of MB dye in detail.

Effect of temperature on adsorption

The effect of temperature on adsorption capacity of *N,O*-CMCTS is shown in Fig. 5. As can be seen, the adsorption capacity of *N,O*-CMCTS increased from 349 to

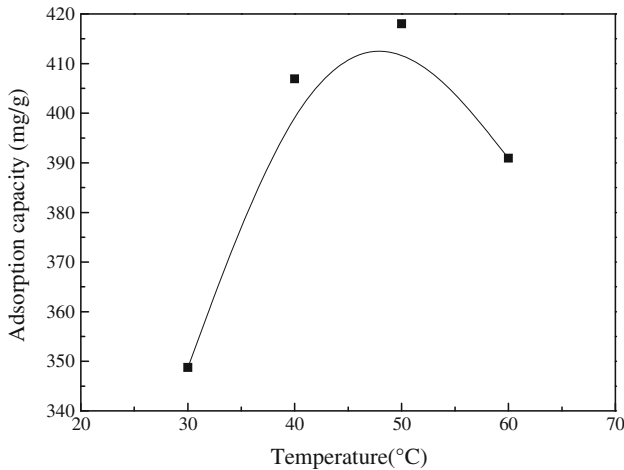


Fig. 5 Effect of the temperature on the adsorption capacities of *N,O*-CMCTS with the DS of 0.76 for MB. Adsorption experiments—dye concentration: 1800 mg/L; sample dose: 0.10 g/25 mL; pH: 8.0; equilibrium time: 60 min

418 mg/g with increasing temperature from 30 to 50 °C, indicating that higher temperature facilitates the adsorption of MB on *N,O*-CMCTS. This may be attributed to the fact that *N,O*-CMCTS is partly swollen at higher temperature, which helps penetration of dye molecules into the interlayer space of *N,O*-CMCTS [31]. However, with further increasing temperature from 50 to 60 °C, the adsorption capacity of *N,O*-CMCTS decreased from 418 to 391 mg/g. The mobility of the large dye ions increases with increasing temperature, which is responsible for the decrease of adsorption capacity of *N,O*-CMCTS.

Adsorption kinetics

Figure 6 shows the effect of time on the adsorption behavior of MB by *N,O*-CMCTS. As can be seen, the adsorption capacity of MB on *N,O*-CMCTS increased sharply with increasing adsorption time, and then slowly increased after 15 min. Maximum adsorption of MB on *N,O*-CMCTS was observed at 60 min. Thus, adsorption time of 60 min was chosen to ensure equilibrium was reached under our experimental conditions.

To investigate the potential rate-controlling steps involved in the adsorption of MB onto *N,O*-CMCTS, both pseudo-first-order and pseudo-second-order kinetic models were used to fit the experimental data.

The pseudo-first-order rate expression of Lagergren model [32] is generally expressed as follows:

$$\frac{dq_e}{dt} = k_1(q_e - q_t) \quad (1)$$

After integration with the initial condition $q_t = 0$ at $t = 0$, Eq. 2 can be obtained

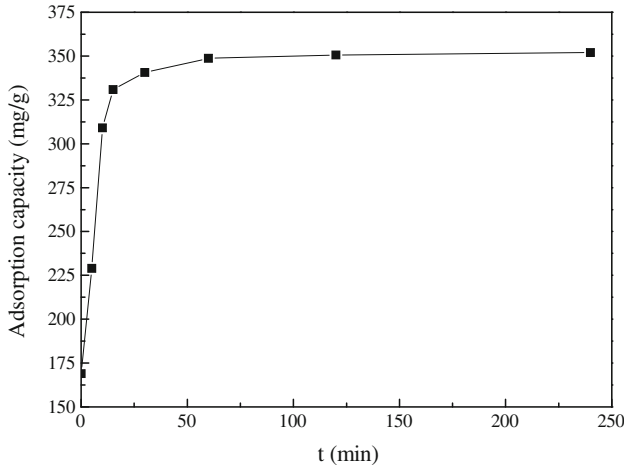


Fig. 6 Effect of the adsorption time on adsorption capacity of *N,O*-CMCTS with the DS of 0.76 for MB. Adsorption experiments—dye concentration: 1600 mg/L; sample dose: 0.10 g/25 mL; pH: 8.0; temperature: 30 °C

$$\log(q_e - q_t) = \log q_e - \frac{k_1 t}{2.303} \tag{2}$$

The pseudo-second-order rate equation is given as [33]

$$\frac{t}{q_t} = \frac{1}{k_2 q_e^2} + \frac{t}{q_e} \tag{3}$$

where q_e and q_t are the amounts of adsorption dye (mg/g) at equilibrium and at time t (min), k_1 (min^{-1}) and k_2 ($\text{g mg}^{-1} \text{min}^{-1}$) are the adsorption rate constant of pseudo-first-order, pseudo-second-order adsorption rate, respectively. The linear plots of $\log(q_e - q_t)$ versus t and (t/q_t) versus t are drawn for the pseudo-first-order and the pseudo-second-order models, respectively. The rate constants k_1 and k_2 can be obtained from the plot of experimental data.

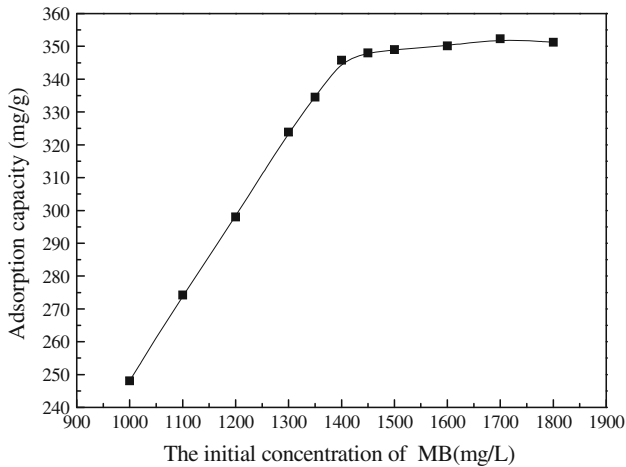
The rate constants, the correlation coefficients, and the calculated q_e of the two kinetic models are shown in Table 2. The correlation coefficients (R^2) of the pseudo-first-order and pseudo-second-order models are 0.9151 and 0.9999, respectively. In addition, the calculated q_e values of the pseudo-first-order and pseudo-second-order models for the adsorption of MB by *N,O*-CMCTS were 53 mg/g and 353 mg/g, respectively. Obviously, the calculated q_e value agreed with the experimental data (349 mg/g) in the case of the pseudo-second-order model. It is clear that the adsorption of MB on *N,O*-CMCTS followed the pseudo-second-order rather than the pseudo-first-order model.

Adsorption isotherms

Figure 7 shows the influence of initial dye concentration on adsorption capacity of *N,O*-CMCTS. It is clear that initial dye concentration is an important factor

Table 2 The rate constants, the correlation coefficients and the calculated q_e of the two kinetic models

Samples	Pseudo-first-order model			Pseudo-second-order model		
	$k_1 (\times 10^{-2} \text{ min}^{-1})$	R^2	q_e	$k_2 (\times 10^{-4} \text{ g/mg/min})$	R^2	q_e
<i>N,O</i> -CMCTS	3.45	0.9151	53	2.34	0.9999	353

**Fig. 7** Effect of the initial dye concentration on the adsorption capacities of *N,O*-CMCTS with the DS of 0.76 for MB. Adsorption experiments—sample dose: 0.10 g/25 mL; pH: 8.0; temperature: 30 °C; equilibrium time: 60 min

affecting adsorption capacity of *N,O*-CMCTS. As shown in Fig. 7, the adsorption capacity of the *N,O*-CMCTS sharply increased from 248 to 349 mg/g with increasing dye concentration from 1000 to 1450 mg/L, and remained almost constant with further increasing dye concentration.

Adsorptions isotherms are important for the description of how molecules of adsorbate interact with adsorbent surface. Hence, the correlation of equilibrium data using either a theoretical or empirical equation is essential for the adsorption interpretation and prediction of the extent of adsorption [34]. The equilibrium adsorption data were generally interpreted using Langmuir and Freundlich models [35], which are represented by the following equations, respectively:

$$\frac{C_e}{q_e} = \frac{1}{bq_m} + \frac{C_e}{q_m} \quad (4)$$

$$q_e = K_f C_e^{1/n} \quad (5)$$

where q_m (mg/g) and b (L/mg) are Langmuir isotherm coefficients. The value of q_m represents the maximum adsorption capacity. K_f (mg/g) and n are Freundlich constants. Two adsorption isotherms were constructed by plotting the C_e/q_e versus C_e , $\log q_e$ versus $\log C_e$, respectively.

The values of R^2 of Langmuir and Freundlich models are 0.9999 and 0.8864, respectively. In addition, the q_m value for the adsorption of MB by *N,O*-CMCTS was 351 mg/g, which are same as the experiment data 350 mg/g for *N,O*-CMCTS. It can be seen that the adsorption of MB is in good agreement with the Langmuir isotherm rather than the Freundlich isotherm. This indicates that the surface of *N,O*-CMCTS was covered by the monolayer of MB molecules. Similar behavior was also found for the adsorption of MB onto precursor and quaternary ammonium compounds-modified montmorillonite [36], clay [37], Cu(II)-exchanged montmorillonite [38, 39].

Adsorption mechanism of MB dye

FTIR analysis

Figure 8 shows FTIR spectra of *N,O*-CMCTS before (a) and after (b) dye adsorption. The major differences are as follows. The absorption band at 3423 cm^{-1} (Fig. 8a), corresponded to the stretching vibration of O–H and N–H groups was broadened, weakened, and shifted to the lower wave number (3401 cm^{-1}) after the adsorption of MB (Fig. 8b). The bands at 1600 and 1412 cm^{-1} (Fig. 8a), assigned to the asymmetric and symmetric stretching vibration of COO^- , disappeared after adsorption (Fig. 8b). The absorption band at 1081 cm^{-1} (Fig. 8a), attributed to the stretching vibration of the second –OH group, was weakened and shifted to lower wave number (1055 cm^{-1}) (Fig. 8b). At the same time, the bands at 1490 , 1387 , 1329 cm^{-1} , attributed to aromatic skeletal vibrations of MB, appeared after adsorption (Fig. 8b). The bands at 883 , 826 , 665 cm^{-1} , assigned to characteristic adsorption of aromatic skeletal groups of MB, also appeared after adsorption (Fig. 8b). The FTIR analysis results suggest that the –OH, – NH_2 , and –COOH groups of *N,O*-CMCTS were involved in the adsorption process.

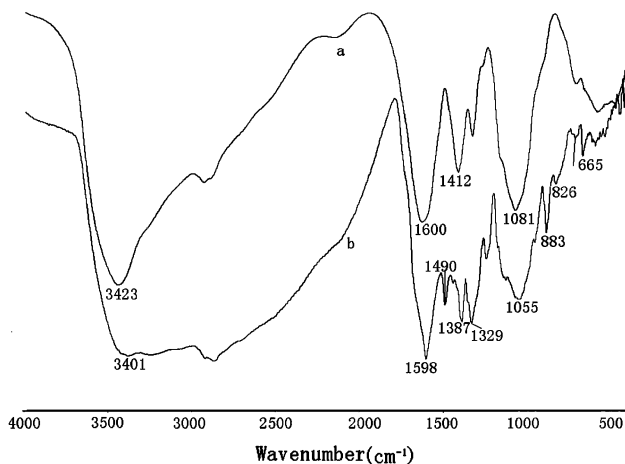


Fig. 8 FTIR spectra of *N,O*-CMCTS before (a) and after (b) dye adsorption

XPS analysis

The XPS spectra of C 1s, N 1s, O 1s, and S 2p of *N,O*-CMCTS before and after MB adsorption were shown in Fig. 9. It can be seen from this figure that the relative intensity of the O 1s spectrum was weakened after adsorption. This may be due to the fact that the –OH, and –COOH groups of *N,O*-CMCTS were involved in the adsorption process, which leads to the decrease of the oxygen content. However, the relative intensity of the N 1s spectrum was strengthened after adsorption. This may be attributed to the adsorption of dye and plentiful nitrogen contained in the MB dye molecule, which leads to the increase of the nitrogen content. At the same time, the new peaks of C 1s spectrum at the binding energy (BE) of 285.71 eV and S 2p spectrum at the binding energy (BE) of 164.21 and 168.21 eV appear after adsorption, which may be attributed to the adsorption of dye and plentiful carbon and sulfur contained in the MB dye molecule.

It also can be seen from Fig. 9 that the BE of C 1s increased from 285.02 to 285.24 eV after adsorption. In addition, the BE of N 1s decreased from 399.61 to 399.23 eV, while the BE of O 1s decreased from 531.72 to 530.95 eV after adsorption. Evidently, carbon atom provides electron pair, nitrogen and oxygen

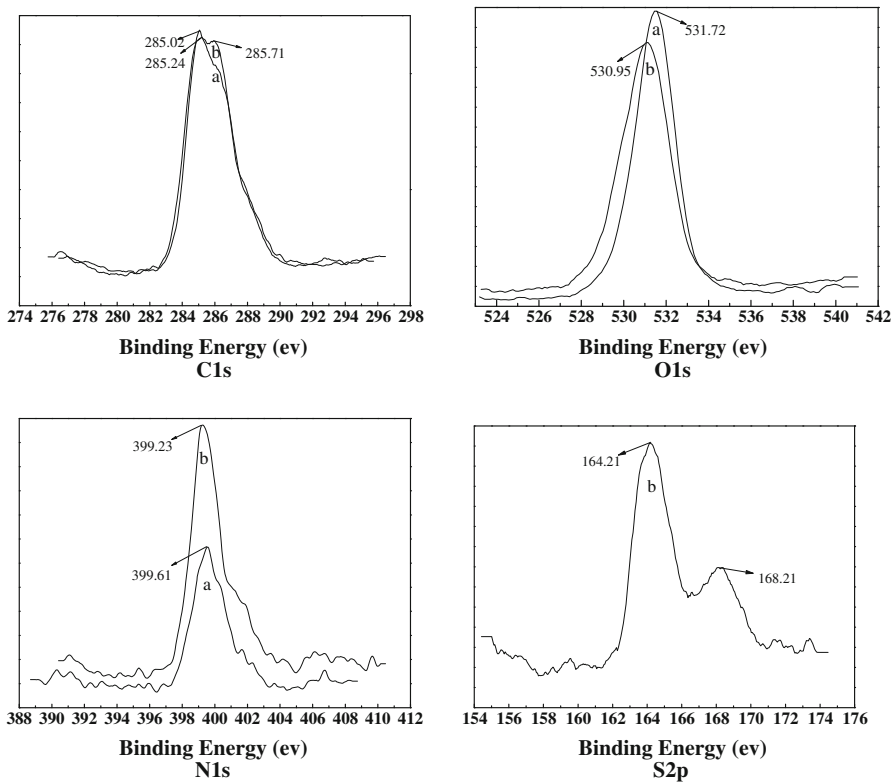


Fig. 9 XPS spectra of *N,O*-CMCTS before (a) and after (b) dye adsorption

atom is inclined to accept the electron. This further implied that the $-OH$, $-NH_2$, and $-COOH$ groups of *N,O*-CMCTS were involved in the adsorption process. The explanations for the adsorption mechanism of MB dye on *N,O*-CMCTS are in good agreement with the FTIR analysis.

Desorption of MB

Desorption studies can help elucidate the mechanism of an adsorption process. If the dye adsorbed onto the adsorbent can be desorbed by water, it can be concluded that the attachment of the dye onto the adsorbent is by weak bonds. If the strong acids, such as HCl can desorb the dye, it can be concluded that the adsorption of the dye onto the adsorbent is by ion exchange or electrostatic attraction [30]. Effect of pH on desorption percentage of dye from dye-loaded *N,O*-CMCTS is shown in Fig. 10. Apparently, the desorption percentage of *N,O*-CMCTS decreased sharply with increasing the pH of distilled water. The lowest desorption was obtained at pH 9.0 and the desorption percentage for *N,O*-CMCTS was only 2.1%, while in the case of pH 2.0, 42.8% was obtained. The fact that the high desorption occurred at pH 2.0 suggested that the adsorption of MB onto *N,O*-CMCTS is mainly via electrostatic attraction, which further substantiated the discussion of the effect of the pH on adsorption. These results indicated that *N,O*-CMCTS provided the potential for regeneration and reuse after MB dye adsorption despite 57.2% dye remaining in the adsorbent in the case of pH 2.0. In addition, the spent *N,O*-CMCTS can be used as a fuel due to its high-polymer content and the bottom ash after its combustion/incineration can be blended with clay/cement-concrete mixture to make bricks and building blocks for its safe disposal [39]. Thus, *N,O*-CMCTS can be used as an alternative-adsorbing agent in dye wastewaters.

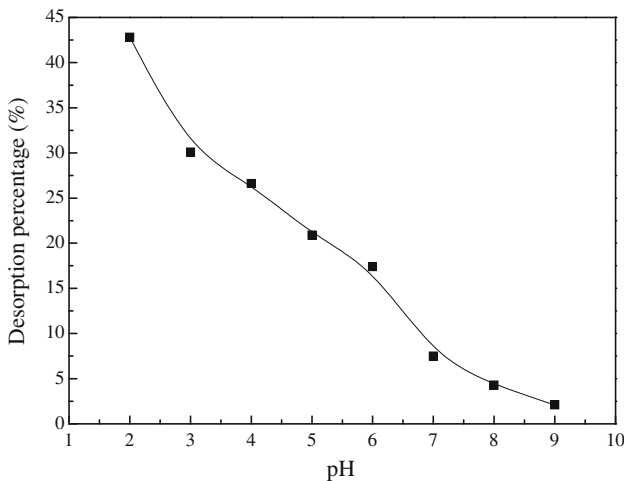


Fig. 10 Effect of pH on desorption percentage of dye from dye-loaded *N,O*-CMCTS with the DS of 0.76. Adsorption experiments—dye concentration: 1600 mg/L; sample dose: 0.10 g/25 mL; pH: 8.0; temperature: 30 °C; equilibrium time: 60 min

Conclusion

N,O-carboxymethyl-chitosans (*N,O*-CMCTS) has been prepared under heterogeneous conditions by controlling the reaction time. Adsorption tests of MB dye on *N,O*-CMCTS were carried out and the results obtained from this study showed that *N,O*-CMCTS with DS of 0.72 exhibited the highest adsorption capacity. The kinetics and isotherm studies indicated that the pseudo-second-order model and the Langmuir model well described the adsorption equilibrium of MB on *N,O*-CMCTS. The FTIR and XPS analysis results suggested that the adsorption site of *N,O*-CMCTS may be not only on –COOH but also on the –NH₂ and –OH. The desorption studies showed that *N,O*-CMCTS is a promising biosorbent for dye removal from MB dye wastewater.

Acknowledgments The authors thank for jointly supporting by Natural Science Foundation of Inner Mongolia Autonomous Region of China (No. 20080404MS0608) and Taihu Project of Jiangsu Provincial Science and Technology Office (No. BS2007118).

References

1. Wu TX, Lin T, Zhao JC, Hidaka H, Serpone N (1999) TiO₂-assisted photodegradation of dyes. 9. Photooxidation of a squarylium cyanine dye in aqueous dispersions under visible light irradiation. *Environ Sci Technol* 33:1379–1387
2. Annadurai G, Krishnan MRV (1997) Batch equilibrium adsorption of reactive dye onto natural biopolymer. *Iran Polym J* 6:169–175
3. Chiou MS, Chuang GS (2006) Competitive adsorption of dye metanil yellow and RB15 in acid solutions on chemically cross-linked chitosan beads. *Chemosphere* 62:731–740
4. Panswed J, Wongchaisuwana S (1986) Mechanism of dye wastewater color removal by magnesium carbonate-hydrated basic. *Water Sci Technol* 18:139–144
5. Ciardelli G, Corsi L, Marucci M (2000) Membrane separation for wastewater reuse in the textile industry. *Resour Conserv Recycl* 31:189–197
6. Purkait MK, DasGupta S, De S (2006) Micellar enhanced ultrafiltration of eosin dye using hexadecyl pyridinium chloride. *J Hazard Mater B* 136:972–977
7. Swaminathan K, Sandhya S, Carmalin SA, Pachhade K, Subrahmanyam YV (2003) Decolorization and degradation of H-acid and other dyes using ferrous–hydrogen peroxide system. *Chemosphere* 50:619–625
8. Muthukumar M, Selvakumar N (2004) Studies on the effect of inorganic salts on decolouration of acid dye effluents by ozonation. *Dyes Pigments* 62:221–228
9. Alinsafi A, Khemis M, Pons MN, Leclerc JP, Yaacoubi A, Benhammou A, Nejmeddine A (2005) Electro-coagulation of reactive textile dyes and textile wastewater. *Chem Eng Process* 44:461–470
10. Mall ID, Srivastava VC, Agarwal NK, Mishra IM (2005) Removal of Congo red from aqueous solution by bagasse fly ash and activated carbon: kinetic study and equilibrium isotherm analyses. *Chemosphere* 61:492–501
11. Purkait MK, Maiti A, DasGupta S, De S (2007) Removal of Congo red using activated carbon and its regeneration. *J Hazard Mater B* 145:287–295
12. Allen SJ (1996) Types of adsorbent materials. In: McKay G (ed) *Use of adsorbents for the removal of pollutants from wastewaters*. CRC Press, Boca Raton, pp 59–97
13. Chang MY, Juang RS (2004) Adsorption of tannic acid, humic acid, and dyes from water using the composite of chitosan and activated clay. *J Colloid Interface Sci* 278:18–25
14. Vieira RS, Beppu MM (2006) Interaction of natural and crosslinked chitosan membranes with Hg(II) ions. *Colloids Surf A* 279:196–207
15. Juang RS, Ju CY (1997) Equilibrium sorption of Copper(II)-ethylenediaminetetraacetic acid chelates onto cross-linked, polyaminated chitosan beads. *Ind Eng Chem Res* 36:5403–5409

16. Crini G (2006) Non-conventional low-cost adsorbents for dye removal: a review. *Bioresour Technol* 97:1061–1085
17. Sherbiny IME (2009) Synthesis, characterization and metal uptake capacity of a new carboxymethyl chitosan derivative. *Eur Polym J* 45:199–210
18. Sugimoto M, Morimoto M, Sashiwa H, Saimoto H, Shigemasa Y (1998) Preparation and characterization of water-soluble chitin and chitosan derivatives. *Carbohydr Polym* 36:49–59
19. Sashiwa H, Shigemasa Y (1999) Chemical modification of chitin and chitosan 2: preparation and water soluble property of *N*-acetylated partially deacetylated chitins. *Carbohydr Polym* 39:127–138
20. Terada N, Morimoto M, Saimoto H, Okamoto Y, Minami S, Shigemasa Y (1999) Synthesis of water-soluble oxidized chitosan derivatives and their biological activity. *Chem Lett* 28:1285–1292
21. Sridhari TR, Dutta PK (2000) Synthesis and characterization of maleilated chitosan for dye house effluent. *Indian J Chem Technol* 7:198–201
22. Heras A, Rodriguez NM, Ramos VM, Agulló E (2001) *N*-Methylene phosphonic chitosan: a novel soluble derivative. *Carbohydr Polym* 44:1–8
23. Choong J, Wolfgang HH (2003) Chemical modification of chitosan and equilibrium study for mercury ion removal. *Water Res* 37:4770–4780
24. Hon NS, Tang LG (2000) Chelation of chitosan derivatives with zinc ions.I. *O,N*-carboxymethyl. *J Appl Polym Sci* 77:2246–2253
25. Sun SL, Wang AQ (2006) Adsorption kinetic of Cu(II) ions using *N,O*-carboxymethyl-chitosan. *J Hazard Mater B* 131:103–111
26. Ngah WSW, Liang KH (1999) Adsorption of gold(III) ions onto chitosan and *N*-carboxymethyl chitosan: equilibrium studies. *Ind Eng Chem Res* 38:1411–1414
27. Wang L, Wang AQ (2008) Adsorption properties of Congo red from aqueous solution onto *N,O*-carboxymethyl-chitosan. *Bioresour Technol* 99:1403–1408
28. Lu SJ, Song X, Cao D (2004) Preparation of water-soluble chitosan. *J Appl Polym Sci* 91:3497–3503
29. Balistrieri LS, Murray JW (1981) The surface chemistry of goethite (α -FeOOH) in major ion seawater. *Am J Sci* 281:788–806
30. Mall ID, Srivastava VC, Kumar GVA, Mishra IM (2006) Characterization and utilization of mesoporous fertilizer plant waste carbon for adsorptive removal of dyes from aqueous solution. *Colloids Surf A* 278:175–187
31. Bhattacharyya KG, Sarma A (2003) Adsorption characteristics of the dye, brilliant green, on neem leaf powder. *Dyes Pigments* 57:211–222
32. Lagergren S (1898) About the theory of so-called adsorption of soluble substances. *Handlingar* 24:1–39
33. Ho YS, McKay G (1999) Pseudo-second order model for sorption processes. *Process Biochem* 34:451–465
34. Grabowska EL, Gryglewicz G (2007) Adsorption characteristics of Congo red on coal-based mesoporous activated carbon. *Dyes Pigments* 74:34–40
35. Periasamy K, Namasivayam C (1995) Removal of Nickel(II) from aqueous solution and nickel plating industry wastewater industry using an agriculture waste: peanut hull. *Waste Manag* 15:63–68
36. Wibulswas R (2004) Batch and fixed bed sorption of methylene blue on precursor and QACs modified montmorillonite. *Sep Purif Technol* 39:3–12
37. Gürses A, Karaca S, Doğan Ç, Bayrak R, Açıkyıldız M, Yalçın M (2004) Determination of adsorptive properties of clay/water system: methylene blue sorption. *J Colloid Interface Sci* 269:310–314
38. Ma YL, Xu ZR, Guo T, You P (2004) Adsorption of methylene blue on Cu (II)-exchanged montmorillonite. *J Colloid Interface Sci* 280:283–288
39. Wang L, Zhang JP, Wang AQ (2008) Removal of methylene blue from aqueous solution using chitosan-g-poly (acrylic acid)/montmorillonite superadsorbent nanocomposite. *Colloids Surf A* 322:47–53